Inorganic Chemistry

Article

pubs.acs.org/IC

Syntheses and Characterization of Nine Quaternary Uranium Chalcogenides Among the Compounds $A_2M_3UQ_6$ (A = K, Rb, Cs; M = Pd, Pt; Q = S, Se)

George N. Oh,[†] Eun Sang Choi,[‡] and James A. Ibers[†,*]

[†]Department of Chemistry, Northwestern University, 2145 Sheridan Road, Evanston, Illinois 60208-3113, United States

[‡]Department of Physics and the National High Magnetic Field Laboratory, Florida State University, Tallahassee, Florida 32310, United States

Supporting Information

ABSTRACT: Nine compounds from the series $A_2M_3UQ_6$ (A = K or Rb or Cs; M = Pd or Pt; Q = S or Se) were synthesized by reacting U, M, and Q in ACl or A_2Q_x fluxes. These compounds crystallize with eight formula units in the $NaBa_2Cu_3O_6$ structure type, in space group *Fmmm* of the orthorhombic system. The structure contains hexagons formed from six edge-sharing square-planar coordinated M atoms, which in turn edge-share with trigonal-prismatically coordinated U atoms, forming layers along (010). These layers are separated by A atoms. Electrical resistivity measurements along the [100] direction of $Rb_2Pd_3US_6$ show typical semiconductor behavior. Magnetic susceptibility measurements on $Rb_2Pd_3US_6$ display marked magnetic anisotropy and unusually low magnetic moments owing to crystalline electric field effects.

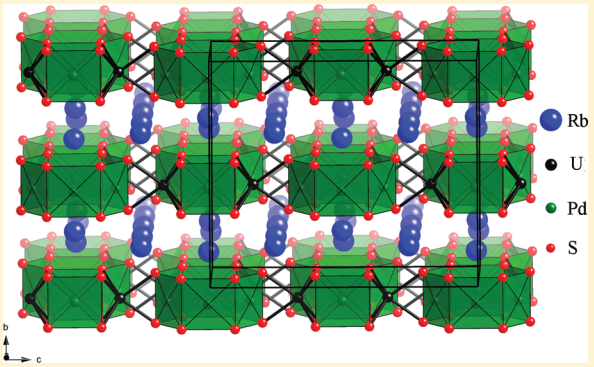

INTRODUCTION

In compounds containing an actinide and a transition metal, magnetic properties are complicated by interactions between *f*-orbital electrons of the actinide and valence orbitals of the transition metal. These atoms are in close proximity in intermetallic compounds, generally resulting in orbital overlap. Incorporating an anion such as a chalcogenide results in the formation of structures where the magnetic atoms are further apart. An added benefit is that oxidation states can be more easily assigned to the atoms, as the atoms adopt characteristic coordination environments that are not seen in intermetallic compounds.

Many ternary transition-metal uranium chalcogenides have been reported in the literature, but there are relatively few such quaternary compounds. We have recently reviewed some of these compounds[1] and have since reported the compounds $Tl_3Cu_4USe_6$,[2] $Tl_2Ag_2USe_4$,[2] and $Ba_8Hg_3U_3S_{18}$.[3] In these quaternary compounds the transition metal is coordinated tetrahedrally by chalcogen atoms with the following exceptions: $Ba_8Hg_3U_3S_{18}$ (linear); $CsMUTe_5$ (M = Ti, Zr)[4] and $Ba_4Cr_2US_9$[5] (octahedral); $Cs_8Hf_5UTe_{30.6}$[6] (trigonal prismatic); and $K_6Cu_{12}U_2S_{15}$[7] (trigonal planar).

Pd and Pt preferentially adopt square-planar coordination environments; thus, reaction of these metals with actinides such as U can result in compounds with structures that differ from those above. Whereas there are no examples of ternary compounds containing Pt, U, and Q (Q = S, Se, or Te) in the literature, several Pd-containing ternary compounds have been reported. $Pd_3U_{0.9}S_4$ displays complex magnetism that has been modeled with mixed-valent U and Pd and a strong temperature-independent magnetic susceptibility contribution.[8,9] $PdUSe_3$ crystallizes in a modified perovskite structure. The only magnetic contribution is from U^{4+}, and the compound orders antiferromagnetically, once again with a strong temperature-independent magnetic susceptibility contribution.[10] Both of these compounds contain square-planar coordinated Pd. Pd_2US_4 also contains square-planar coordinated Pd, and U may be assigned the tetravalent oxidation state from charge-balance arguments.[8] The Pd atom in PdU_2S_4 is coordinated in a sawhorse manner. No magnetic susceptibility measurements were reported for Pd_2US_4 or PdU_2S_4.

To explore further this diversity in physical properties and chemistry, we have examined quaternary systems containing an alkali metal, a platinum metal, uranium, and a chalcogen. We previously reported the new layered compound $Cs_2Pd_3USe_6$,[11] and here we present the syntheses and characterization of it and some other members of the isostructural series $A_2M_3UQ_6$ (A = K or Rb or Cs; M = Pd or Pt; Q = S or Se).

EXPERIMENTAL METHODS

Syntheses. U filings (Oak Ridge National Laboratory) were powdered by hydridization and subsequent decomposition under heat and vacuum,[12] in a modification of a previous literature method.[13] A_2Q and A_2Q_3 fluxes were synthesized by the stoichiometric reactions of

Received: December 15, 2011
Published: March 16, 2012

ACS Publications © 2012 American Chemical Society

Table 1. Crystallographic Details[a]

	fw (g mol^{-1})	a (Å)	b (Å)	c (Å)	V (Å^3)	ρ_c (g cm^{-3})	μ (mm^{-1})	$R(F)$[b]	$R_w(F_o^2)$[c]	q[c]
$Cs_2Pt_3USe_6$	1562.88	10.0904(5)	15.3859(7)	17.5882(8)	2730.6(2)	7.603	63.670	0.0198	0.0391	0.0123
$Cs_2Pt_3US_6$[d]	1281.48	9.7924(8)	14.8937(8)	17.016(2)	2481.8(3)	6.859	53.463	0.0259	0.0664	0.0226
$Cs_2Pd_3USe_6$	1296.81	10.1034(5)	15.5046(8)	17.5503(8)	2749.2(2)	6.266	36.665	0.0194	0.0545	0.0241
$Cs_2Pd_3US_6$[d]	1015.41	9.7874(4)	15.0077(4)	16.9773(7)	2493.7(2)	5.409	23.910	0.0247	0.0629	0.0293
$Rb_2Pt_3USe_6$	1468.00	10.0467(1)	14.7961(1)	17.4663(2)	2594.64(4)	7.516	68.930	0.0194	0.0386	0.0137
$Rb_2Pt_3US_6$	1186.60	9.755(1)	14.229(1)	16.897(2)	2345.5(4)	6.721	58.698	0.0155	0.0434	0.0107
$Rb_2Pd_3USe_6$	1201.93	10.0525(3)	14.8432(5)	17.4127(5)	2598.2(1)	6.145	40.718	0.0214	0.0656	0.0224
$Rb_2Pd_3US_6$	920.53	9.7462(2)	14.3306(2)	16.8572(3)	2354.43(7)	5.194	27.445	0.0236	0.059	0.0234
$K_2Pd_3US_6$[d]	827.79	9.7265(5)	13.8721(6)	16.7541(8)	2260.4(2)	4.865	20.765	0.0501	0.1327	0.100

[a]For all structures, T = 100(2) K; λ = 0.71073 Å; Z = 8; space group D_{2h}^{23} − $Fmmm$. [b]$R(F) = \sum||F_o| - |F_c||/\sum|F_o|$ for $F_o^2 > 2\sigma(F_o^2)$. [c]$R_w(F_o^2) = \{\sum w(F_o^2 - F_c^2)^2/\sum wF_o^4\}^{1/2}$. For $F_o^2 < 0$, $w^{-1} = \sigma^2(F_o^2)$; for $F_o^2 \geq 0$, $w^{-1} = \sigma^2(F_o^2) + (qF_o^2)^2$. [d]Refined as twilled structures.

the appropriate following elements in liquid ammonia at 194 K:[14] Cs (Aldrich, 99.5%), Rb (Strem, 99%), K (Cerac, 98%), S (Mallinckrodt, 99.6%), and Se (Cerac, 99.999%). All other reagents were used as obtained: Pd (Johnson Matthey, 99.94%), Pt wire (Omega Engineering, 0.01 in. diameter, 99.95%), KCl (Aldrich, 99%+), and CsCl (Aldrich, 99.9%).

All reactants were loaded into 6 mm outer-diameter carbon-coated fused-silica tubes in an argon-filled glovebox, moved to a high-vacuum line, then flame-sealed under 10^{-3} Torr vacuum. They were then placed in a computer-controlled furnace and heated according to the heating profiles detailed below. All compounds are black and air stable. They were cleaned with water. The crystals grow as hexagonal thin plates and thicker prisms. The plates are sturdy and cleave evenly along the three hexagonal edges. The prisms break evenly normal to the hexagonal faces, but cutting across the hexagonal faces of a crystal causes it to fray into plates, which are ductile and may be peeled off. These prisms are polysynthetically twilled, that is, comprise three "twin" domains. EDS analysis on single crystals using a Hitachi S-3400 SEM indicated the presence of only the four elements appropriate for each compound. In all reactions, the primary side product was β-UQ_2.[15,16]

$Cs_2Pd_3USe_6$. Small black plates of $Cs_2UPd_3Se_6$ were initially synthesized as previously reported, using CsCl as a flux.[11] A mixture of Cs_2Se_3 (0.126 mmol), U (0.126 mmol), Pd (0.378 mmol), and excess Se (0.756 mmol) was heated to 1273 K in 96 h, left for 6 h, cooled to 1223 K in 12 h, left for 24 h, cooled to 873 K in 96 h, then to 523 K in 96 h, and finally to 298 K in 24 h. Small hexagonal prisms in approximately 50 wt % yield by U resulted, along with large amounts of black-turquoise hexagons, identified as $Cs_2Pd_3Se_4$.[17]

$Cs_2Pd_3US_6$. A mixture of Cs_2S_3 (0.252 mmol), U (0.126 mmol), Pd (0.378 mmol), and S (1.512 mmol) was heated to 1273 K in 120 h, left for 6 h, cooled to 1223 K in 12 h, left for 24 h, and then cooled to 298 K in 280 h, yielding hexagonal prisms in about 40 wt % yield.

$Cs_2Pt_3USe_6$. A mixture of Cs_2Se_3 (0.126 mmol), U (0.126 mmol), Pt (0.378 mmol), and Se (0.630 mmol) was heated to 1273 K in 96 h, held there for 6 h, cooled to 1223 K in 12 h, held there for 24 h, and then cooled to 298 K in 288 h, yielding hexagonal plates in 20 wt % yield. Side products included clusters of black hexagonal $PtSe_2$ crystals.[18]

$Cs_2Pt_3US_6$. A mixture of Cs_2S_3 (0.126 mmol), U (0.126 mmol), Pt (0.126 mmol), and S (0.504 mmol) was heated according to the profile used for $Cs_2Pt_3USe_6$, yielding triangular and hexagonal plates in 20 wt % yield, along with large clusters of black hexagonal PtS_2 crystals.[18]

$Rb_2Pd_3USe_6$. A mixture of Rb_2Se_3 (0.252 mmol), U (0.126 mmol), Pd (0.378 mmol), and Se (1.512 mmol) was heated to 1173 K in 96 h, left for 192 h, cooled to 873 K in 96 h, and then to 298 K in 96 h, to afford intergrown hexagonal plates and prisms in about 50 wt % yield. Crystals were washed with a mixture of water and DMF. Some prisms were fragile and especially prone to splitting into thinner plates. A sturdy hexagonal prism was selected for X-ray diffraction experiments.

$Rb_2Pd_3US_6$. A mixture of Rb_2S_3 (0.252 mmol), U (0.126 mmol), Pd (0.378 mmol), and S (1.512 mmol) was heated according to the profile used for $Cs_2Pd_3US_6$ to afford several large black hexagonal prisms and plates and many smaller truncated hexagonal pyramids in 60 wt % yield. A small crystal was selected for X-ray diffraction experiments, whereas larger crystals were selected for single-crystal anisotropic magnetic susceptibility measurements.

$Rb_2Pt_3USe_6$. A mixture of Rb_2Se_3 (0.126 mmol), U (0.126 mmol), Pt (0.126 mmol), and Se (0.504 mmol) was heated to 1223 K in 96 h, held there for 192 h, cooled to 773 K in 96 h, and then cooled to 298 K in 24 h, yielding hexagonal prisms in 20 wt % yield. A few tapered black needles of $Rb_2Pt_4U_6Se_{17}$[19] were found in the same tube, along with large amounts of $PtSe_2$, also growing in a large rod-like cluster.

$Rb_2Pt_3US_6$. A mixture of Rb_2S_3 (0.126 mmol), U (0.126 mmol), Pt (0.126 mmol), and S (0.504 mmol) was heated according to the profile used for $Rb_2Pt_3USe_6$, yielding hexagonal prisms in 20 wt % yield, along with large amounts of black hexagonal prisms of PtS_2 in the same clusters.

$K_2Pd_3US_6$. A mixture of K_2S (0.126 mmol), U (0.126 mmol), Pd (0.189 mmol), S (0.504 mmol), and KCl (1.386 mmol) was heated according to the profile used for $Rb_2Pt_3USe_6$ to afford hexagonal prisms in 40 wt % yield and tiny black hexagonal $K_2Pd_3S_4$ crystals.[17]

Structure Determinations. Data for $Rb_2Pd_3US_6$, $Rb_2Pt_3US_6$, and $Rb_2Pd_3USe_6$ were collected on a Bruker APEXII KAPPA diffractometer. Data collection strategies composed of ω and ϕ scans were devised using COSMO in APEX2.[20] For $Rb_2Pt_3USe_6$, data were collected on a Bruker APEXII platform diffractometer. A strategy was devised using COSMO in APEX2. For all other compounds, full spheres of data were collected on a Bruker APEXII platform diffractometer. The data consisted of ω scans at ϕ = 0°, 90°, 180°, and 270°. Each scan consisted of 606 frames. For all collections, frames were 0.3° in width, and the initial 50 frames were recollected at the end to check for crystal degradation—none was noted. All collections were taken with a detector distance of 60 mm. Counting times were 10 s/frame for $Cs_2Pt_3USe_6$, $Cs_2Pd_3USe_6$, $Cs_2Pd_3US_6$, $Rb_2Pt_3US_6$, $Rb_2Pd_3US_6$, and $K_2Pd_3US_6$ and 20 s/frame for $Cs_2Pt_3US_6$, $Rb_2Pt_3USe_6$, and $Rb_2Pd_3USe_6$. Cell refinement and data reduction for single crystals were carried out with SAINT in APEX2.[20] Numerical face-indexed absorption corrections were applied using SADABS.[21] Structure determinations were carried out by direct methods with XS and refinements with XL of the SHELX[22] package. Displacement parameters were refined anisotropically. Secondary corrections for extinction were applied for all structures except $Cs_2Pd_3US_6$ and $Cs_2Pt_3US_6$. The atom positions were standardized using STRUCTURE TIDY[23] in PLATON.[24] Twilled crystals were treated identically except that data reductions were carried out with additional domains in SAINT and absorption corrections were carried out numerically with TWINABS.[25] Crystallographic details are given in Table 1, and selected metrical details in Table 2. Additional information is in the Supporting Information.

dx.doi.org/10.1021/ic2027048 | Inorg. Chem. 2012, 51, 4224−4230

Table 2. Selected Interatomic Distances (Å) for $A_2M_3UQ_6$[a]

	U1−Q1·4	U1−Q2·2	M1−Q1·2	M1−Q2·2	M2−Q1·4	A1−Q1·4	A1−Q2·4	A2−Q2·2	A2−Q1·4	A2−Q1·4
$Cs_2Pt_3USe_6$	2.8354(5)	2.8806(7)	2.4582(5)	2.4759(5)	2.4545(5)	3.4557(5)	3.4504(5)	3.7190(7)	3.7607(6)	4.0529(7)
$Cs_2Pt_3US_6$	2.727(1)	2.765(2)	2.346(2)	2.361(2)	2.346(2)	3.365(2)	3.368(2)	3.657(2)	3.699(2)	3.869(2)
$Cs_2Pd_3USe_6$	2.8353(5)	2.8704(2)	2.4557(6)	2.4736(6)	2.4516(5)	3.4653(5)	3.4682(5)	3.7847(7)	3.8301(5)	3.9511(7)
$Cs_2Pd_3US_6$	2.717(1)	2.751(2)	2.346(1)	3.362(1)	2.342(1)	3.377(1)	3.379(1)	3.716(2)	3.758(1)	3.802(1)
$Rb_2Pt_3USe_6$	2.8363(3)	2.8763(5)	2.4614(3)	2.4626(3)	2.4532(3)	3.3429(3)	3.3381(3)	3.6106(5)	3.6738(4)	3.9914(7)
$Rb_2Pt_3US_6$	2.727(1)	2.759(1)	2.349(1)	2.358(1)	2.344(1)	3.243(1)	3.2477(9)	3.563(1)	3.623(1)	3.739(1)
$Rb_2Pd_3USe_6$	2.8331(5)	2.8659(7)	2.4684(5)	2.4560(5)	2.4477(4)	3.3421(4)	3.3462(4)	3.6750(7)	3.7506(5)	3.8244(8)
$Rb_2Pd_3US_6$	2.7178(6)	2.7483(8)	2.3473(6)	2.3571(6)	2.3408(6)	3.2506(6)	3.2573(5)	3.6198(8)	3.6455(7)	3.6864(6)
$K_2Pd_3US_6$	2.715(2)	2.741(2)	2.354(2)	2.353(2)	2.344(2)	3.161(2)	3.176(1)	3.529(2)	3.526(3)	3.658(2)

[a]Atoms have Wyckoff positions and site symmetries as follows: U1 ($i - mm2$); *M*1 ($n - .m.$); *M*2 ($g - 2mm$); *A*1 ($f - 222$); *A*2 ($h - m2m$); *Q*1 ($p - 1$); and *Q*2 ($m - m$).

Magnetic Measurements. Two crystals of $Rb_2Pd_3US_6$ were selected for magnetic measurements. The crystals were washed in DMF and water, and then large surface impurities were mechanically removed under oil. The crystals were rinsed with hexanes, briefly soaked in concentrated HNO_3 to remove smaller impurities, and rinsed with water and then with acetone. The faces were indexed by breaking off a small piece of the crystal and determining the unit cell by X-ray diffraction methods. The crystals, of mass 0.78 mg and 35.4 mg, were in the shape of truncated hexagonal bipyramids. The edges and vertices of the smaller crystal were sharp, typical of an untwilled crystal, whereas the larger crystal had rounded edges and vertices, typical of a twilled crystal.

Magnetic susceptibility measurements were taken by gluing the crystals to a rotating platform. Zero-field-cooled (ZFC) and field-cooled (FC) measurements were identical for each measurement, ruling out ferromagnetic interactions. The core diamagnetism was subtracted using Pascal's law, and the diamagnetic contribution of the sample holder was subtracted by running an identical measurement with an empty sample holder. The susceptibility was measured from 1.8 to 299.9 K in various external fields along each crystallographic axis. Susceptibility vs external field measurements were conducted along all three axes at 5 K. The behavior of the two crystals was identical along the *b* axis. The observed differences in the magnetic behavior along the *a* and *c* axes were more pronounced in the smaller crystal than in the larger crystal, consistent with the twilling of the larger crystal.

Susceptibility data of the smaller crystal taken at external fields of 30 kOe were fit to the modified Curie−Weiss law, $\chi = C/(T - \theta) + \chi_0$, where *C* is the Curie constant, related to the magnetic moment $\mu_{eff} = (8C)^{1/2}$, θ is the Weiss constant, which accounts for magnetic correlations and low-lying crystal-field states, and χ_0 is the temperature-independent paramagnetism, which accounts for itinerancy, or Pauli paramagnetism, and the influence of low-lying crystal-field states, or Van Vleck paramagnetism. Measurements at lower fields yielded unreasonable fits to the modified Curie−Weiss law, owing to large background contributions to the susceptibility from the relatively small crystal. The parameters obtained from these fits are listed in Table 3.

Table 3. Magnetic Behavior of $Rb_2Pd_3US_6$

	b axis (interlayer)	*a* axis (in-layer)	*c* axis (in-layer)
μ_{eff} (μ_B)	3.14	1.8	1.2
θ (K)	1.4	−210	−190
χ_0 (emu mol^{-1} Oe^{-1})	-1.4×10^{-3}	2.7×10^{-3}	1.6×10^{-3}

Electrical Resistivity Measurements. The electrical resistivity of the crystal used in the magnetic measurements was measured with standard four-probe techniques. Four Au wires were attached with carbon paint along the *a* axis. A Keithley 6221 current source and a Keithley 2182 nanovoltmeter were used to measure the resistivity. A total of 50 nA of alternating current was applied using the current source, and the voltage drop was measured using the nanovoltmeter.

DISCUSSION

Syntheses. Nine members of the isostructural series $A_2M_3UQ_6$ (A = K or Rb or Cs; M = Pd or Pt; Q = S or Se) were synthesized at high temperatures using either ACl or A_2Q_3 fluxes. The yields on these reactions were generally good for solid-state reactions, at least 20 wt % by weight U and more often closer to 50 wt %. The ease in which these compounds form and the high temperatures at which they are formed suggest that they are thermodynamically stable. The primary side products are the stable β-UQ_2.[15,16] The clusters of PtQ_2 crystals in the Pt-containing reactions were approximately the same size and shape as the Pt wire starting material. PtS_2 was previously synthesized at temperatures as low as 1098 K and $PtSe_2$ at 873 K.[18] Likely, in the present reactions, the PtQ_2 compounds formed during the initial heating step, and at the maximum reaction temperatures they slowly reacted to form the more stable quaternary products.

We have also synthesized another set of compounds containing the same elements, with formula $A_2M_4U_6Q_{17}$.[19] The syntheses of these compounds occurred at lower reaction temperatures and required A_2Q_3 or ACl fluxes in order to form. This behavior is characteristic of kinetically stable compounds.[26] In instances where both compounds could be synthesized with a given flux, the $A_2M_3UQ_6$ compound required higher temperatures to form. In instances where both could be synthesized at the same temperature, $A_2M_3UQ_6$ and $A_2M_4U_6Q_{17}$ required A_2Q_3 and ACl, respectively.

There are two exceptions: $Rb_2Pt_3USe_6$ and $Rb_2Pt_4U_6Se_{17}$ were found in the same reaction vessel. These formed at a slightly cooler temperature of 1223 K. The yields of the former are higher, as would be expected for reaction conditions closer to those that yield $A_2M_3UQ_6$ in the other compounds. The other exception is $K_2Pd_3US_6$, which required both fluxes to form. Attempts to synthesize $K_2Pd_4U_6S_{17}$ failed.

Structure. The compounds $A_2M_3UQ_6$ crystallize in the $Na-Ba_2Cu_3O_6$ structure type,[27] in which $CaBa_2Pd_3O_6$ also crystallizes.[28] There is no Q−Q bonding, as a typical shortest S···S distance is 3.149(2) Å in $Cs_2Pt_3US_6$, and the shortest Se···Se distance is 3.330(2) Å in $Cs_2Pt_3USe_6$. Charge balance can be achieved by assigning the formal oxidation states as A^+, U^{4+}, M^{2+}, and Q^{2-}.

The defining characteristic of this structure, taking $Rb_2Pd_3US_6$ as an example, is a hexagonal prism formed by six edge-sharing square-planar PdS_4 units. The edges are also shared with trigonal prismatic US_6 units along the three edges common to two rectangular faces. These units form distinct layers along (010) (Figure 1). The layers are staggered by translation of half the unit cell along [100], consistent with

dx.doi.org/10.1021/ic2027048 | Inorg. Chem. 2012, 51, 4224−4230

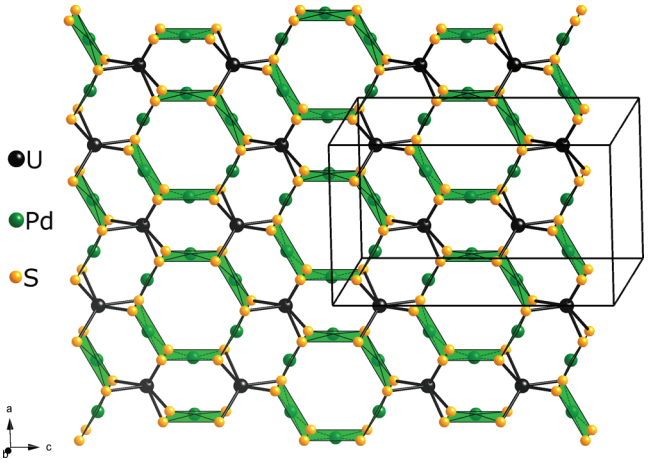

Figure 1. Layer of the structure of $Rb_2Pd_3US_6$ viewed down [010].

the *F* centering of the lattice. The Rb atoms occupy the space between the layers (Figure 2). Atom Rb1 is in a square antiprism, whereas atom Rb2 is ten coordinate, with one hexagonal face and the opposite face square.

Square-planar coordination for Pd^{2+} is typical. Whereas trigonal-prismatic coordination for U^{4+} is less common, it is found in $Ba_4Cr_2US_9$.[5] Interatomic distances in $Rb_2Pd_3US_6$ are typical of these coordination numbers and oxidation states: U−S, 2.7178(6) Å to 2.7483(8) Å vs 2.688(5) Å to 2.764(4) Å in $Ba_4Cr_2US_9$; square-planar Pd1−S, 2.3473(6) Å to 2.3571(6) Å, and Pd2−S, 2.3408(6) Å vs 2.349 Å to 2.365 Å in $Rb_2Pd_3S_4$;[29] eight-coordinate Rb1−S, 3.2506(6) Å to 3.2573(5) Å vs 3.263 Å in $RbCoCuS_2$;[30] and ten-coordinate Rb2−S, 3.6198(8)−3.6864(6) Å vs 3.472(1) Å to 3.775(1) Å in $RbFe_2S_3$.[31] Atom Rb2 has a larger coordination number than atom Rb1 and correspondingly larger displacement parameters and interatomic distances.

The structure of $A_2M_3UQ_6$ is unrelated to those of compounds U/M and U/M/Q but is closely related to those of some of the compounds $A_2M_3Q_4$ (A = K, Rb, Cs; M = Ni, Pd, Pt; Q = S, Se).[17] As an example, the structure of $Cs_2Pd_3Se_4$ comprises layers of $PdSe_4$ units edge-sharing to form a hexagonal lattice, with the Cs atoms lying slightly above and below each layer, in the middle of the hexagons (Figures 3 and 4).

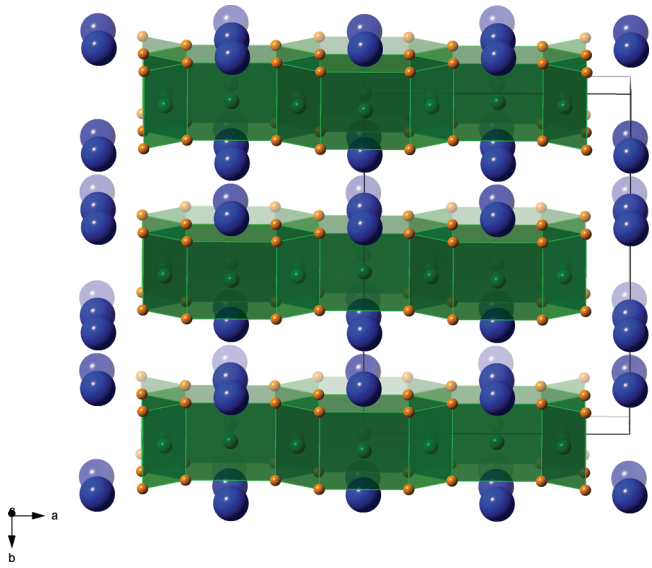

Figure 3. Structure of $Cs_2Pd_3Se_4$ viewed down [001].

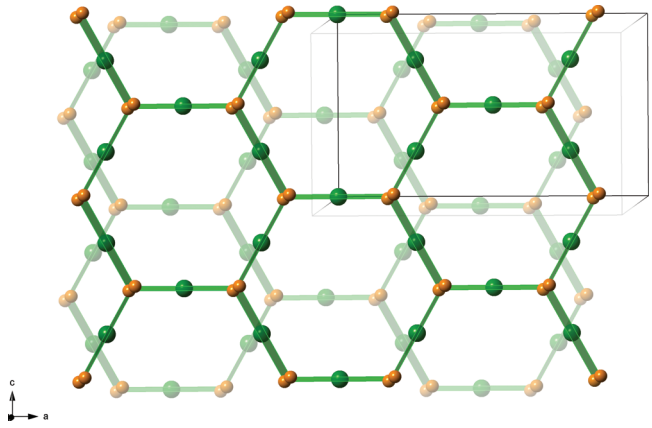

Figure 4. Structure of $Cs_2Pd_3Se_4$ viewed down [010]. Cs atoms are omitted for the sake of clarity.

The present structures are related by insertion of the US_6 polyhedra in the layers, separating the hexagons from each other.

Twilling. Compounds $Cs_2Pt_3US_6$, $Cs_2Pd_3US_6$, and $K_2Pd_3US_6$ were twilled. Twilling occurred in crystals with rounded corners. All twilled crystals were found in reactions

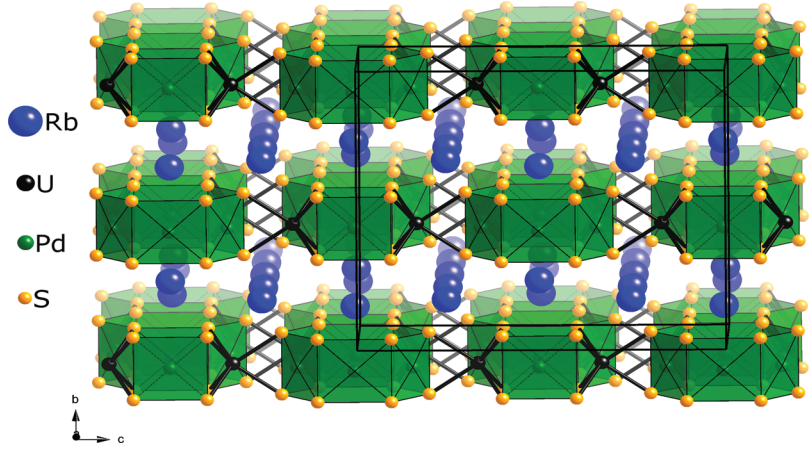

Figure 2. Structure of $Rb_2Pd_3US_6$ viewed down [100].

dx.doi.org/10.1021/ic2027048 | *Inorg. Chem.* 2012, 51, 4224−4230

containing excess A_2Q_x flux. The twin laws for these compounds are

$$\begin{pmatrix} -1/2 & 1/2 & 0 \\ -3/2 & -1/2 & 0 \\ 0 & 0 & 1 \end{pmatrix} \qquad \begin{pmatrix} -1/2 & 1/2 & 0 \\ 3/2 & -1/2 & 0 \\ 0 & 0 & 1 \end{pmatrix}$$

corresponding to 120° and 240° rotations about the *c* axis. As the space group of the structure is orthorhombic, the twin laws are not of the Laue class. However, the symmetry of the structure is pseudohexagonal, with which the twin laws are consistent. For instance, in the untwinned structure of $Rb_2Pd_3US_6$, the angles in the Rb "hexagon" are 119.94(2)° and 120.03(2)° × 2, the S−S−S angles in the US_6 trigonal prism are 58.18(2)° and 60.92(2)° × 2, and the S−S−S angles in the Pd_6S_{12} hexagon are 121.68(2)° and 119.16(2)° × 2. The main divergence from hexagonal symmetry is the displacement of the Rb2 site in the *y* direction, which sits on (0, *y*, 0), in contrast to the Rb1 site which sits on (1/4, 1/4, 1/4). Twilling essentially exchanges the *y* coordinates of Rb1 and Rb2; apparently, it occurs because it does not significantly distort the coordination environments. The reciprocal space lattice is also pseudohexagonal so the twin laws are holohedral with the lattice. This behavior has been treated in depth for other compounds crystallizing in this structure type[32] and may be characterized as "twilling by higher order reticular merohedry."

Systematic Trends. Unsurprisingly, the unit cell axes and cell volumes are smaller for the sulfide compounds than for the corresponding selenide compounds. The cell volumes of Cs compounds are significantly larger than their Rb analogues, but the expansions in the *a* and *c* axes are much smaller than in the *b* axis. Changes in the *a* and *c* axes must be accompanied by distortions in the U and M coordination polyhedra, as the structure layers contain no A atoms. To minimize such distortions, the structure accommodates the larger alkali metal primarily by interlayer expansion along the *b* axis.

The effects of changing M are smaller and less apparent—in all cases, Pd analogues have larger cell volumes than do the corresponding Pt compounds, consistent with the smaller radius of Pt (crystal radius of 0.74 Å vs 0.78 Å for Pd).[33] However, the lengths of the axes change inconsistently, with those of the Pd analogues sometimes being smaller than those of the Pt analogues. Examination of the M−Q distances shows Pt−Q distances are equal to Pd−Q distances to within 0.01 Å, despite the fact that the ionic radius of Pd is 0.04 Å greater than Pt. This is also observed in $Cs_2M_3Se_4$ (Pd−Se: 2.453(6) Å to 2.456(7) Å; Pt−Se: 2.455(14) Å to 2.457(11) Å),[17] and in Na_2MS_2 (Pd−S: 2.35 Å to 2.39 Å; Pt−S: 2.34 Å to 2.38 Å).[34]

Electrical Resistivity. Figure 5 shows the temperature dependence of the electrical resistivity of $Rb_2Pd_3US_6$ along the *a* axis. This dependence is typical for a semiconductor. It may be fit to the Arrhenius formula for thermally activated electrical conductivity, $\rho(T) \propto e^{(E_a/k_BT)}$, where E_a is the activation energy. The slope of the linear fit of ln ρ vs $1/T$ corresponds to E_a = 0.25 eV.

Magnetism. log χ vs log T plots for $Rb_2Pd_3US_6$ are presented in Figure 6, and χ^{-1} vs T plots are given in Figure 7. Examination of the magnetism reveals significant anisotropy when the measurements along the *a* and *c* axes are compared to those along the *b* axis. Additionally, the magnetism exhibits marked divergence from Curie−Weiss behavior, as follows: log χ vs log T plots are linear at high temperatures and (Feature 1) increase more dramatically between 5 to 10 K as seen in curves at low external fields; (Feature 2) at low T, χ shows reduced

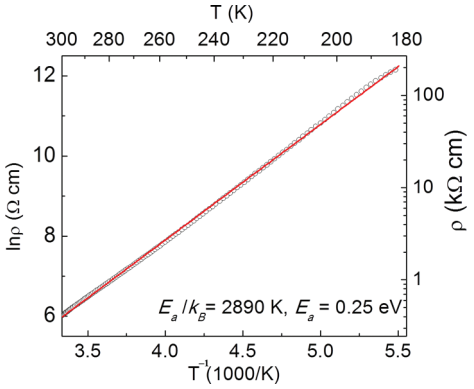

Figure 5. Electrical resistivity ρ versus temperature. Both the linear plot of ln ρ versus T^{-1} (bottom-left) and the nonlinear plot of ρ versus T (top-right) correspond to the curve shown. The solid line corresponds the linear fit of the ln ρ versus T^{-1} plot.

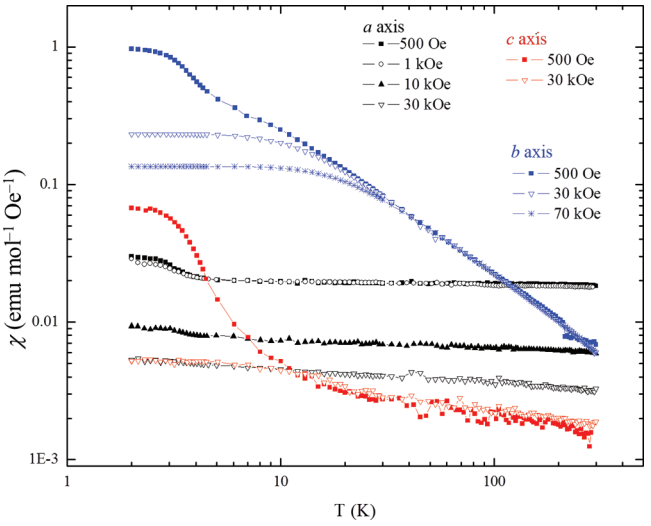

Figure 6. log χ versus log T for $Rb_2Pd_3US_6$ along the three crystallographic axes in various external fields.

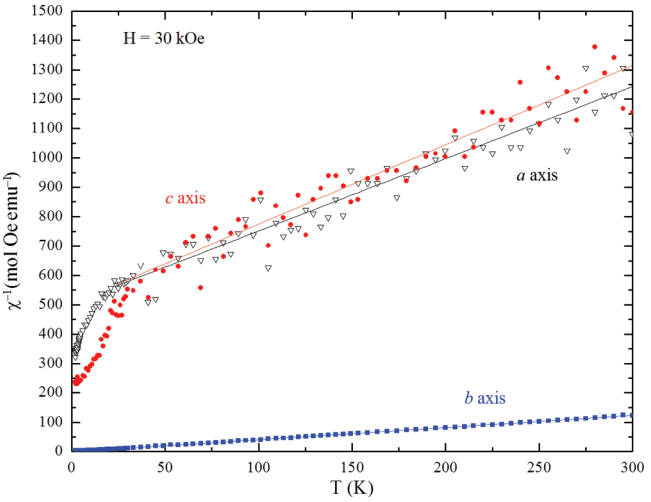

Figure 7. χ^{-1} versus T for $Rb_2Pd_3US_6$. The high temperature portions can be fit to the modified Curie−Weiss law, as indicated by the straight lines.

dependence on T, also seen in $Pd_3U_{0.9}S_4$; (Feature 3) the susceptibility changes as the external field is changed, especially in the *a* axis measurements.

dx.doi.org/10.1021/ic2027048 | Inorg. Chem. 2012, 51, 4224−4230

The susceptibility data at 30 kOe above 50 K have been fit to the modified Curie–Weiss law (Figure 7). The fitting parameters in Table 3 for the *a* and *c* axes are close to one another, but anisotropy is evident when comparing the *b*-axis (interlayer) parameters to the *a* and *c* (in-layer) parameters. These differences are unsurprising given that the layers are well separated by the A atoms and are pseudohexagonal in symmetry. U is the only atom containing unpaired electrons, so magnetic properties are a function of the interatomic U···U distances. U···U distances are 7.6857(1) Å along the *b* axis, but 5.6485(5) Å along the *a* axis and 5.6103(2) Å also in the layer. The interlayer Weiss constant (θ) is close to zero, which suggests that the magnetic properties along the *b* axis are dominated by largely independent magnetic ions, with minimal coupling as a consequence. In contrast, the in-layer Weiss constants of −190 and −210 K are consistent with antiferromagnetic coupling within the layers. Whereas the interlayer temperature-independent term (χ_0) is negative, it is positive in-layer. A positive χ_0 term indicates either Pauli paramagnetism from conduction electrons or ferromagnetic impurities. As $Rb_2Pd_3US_6$ displays semiconductor behavior, Pauli paramagnetism may be ruled out.

The in-layer effective magnetic moments are 1.8 μ_B and 1.2 μ_B, but the magnetic moment of 3.14 μ_B along the *b* (interlayer) axis is closer to the calculated free ion moment of 3.6 μ_B for U^{4+}. Square-planar Pd^{2+} has no unpaired electrons and is diamagnetic. Reduced magnetic moment may be explained by either itinerant 5*f* electrons or crystalline electric field (CEF) effects. Given that $Rb_2Pd_3US_6$ is not metallic, we attribute the reduced magnetic moment to CEF effects. Uranium sits in an isosceles trigonal prismatic coordination environment with site symmetry *mm*2. In this orthorhombic crystal field environment, the $^3H_4$ multiplet of free-ion U^{4+} can be split into several CEF levels. When the thermal energy is smaller than the CEF splitting energy the electrons will not occupy all of the states, resulting in paired electrons and reduced effective magnetic moment. This and the increase in susceptibility beyond normal Curie–Weiss behavior at low temperatures correspond to a splitting energy of 5–10 K (Feature 1). Each CEF level further splits into two sublevels in an external magnetic field owing to the Zeeman effect. Such splitting is typically small, equal to $\mu_{eff}\mathbf{B}$, where **B** is the external magnetic field. In this compound, the Zeeman effect appears to affect the magnetism significantly because of the comparably small CEF splitting energy, leading to magnetic field dependent susceptibility at low temperatures (Feature 3). We decline to fit the low-temperature behavior using the van Vleck formula, as to do this requires full knowledge of the CEF scheme.

Comparison may be made to $Pd_3U_{0.9}S_4$, which has an effective magnetic moment of 2.60–2.71 μ_B/mol U;[9] these are significantly higher than the in-layer values in the present compound but lower than the free-ion moment. The coordination environment of U in $Pd_3U_{0.9}S_4$ is cubic; the reduction in μ_{eff}, which is also attributed to CEF effects, is less dramatic.

Another feature of note is the reduced $\chi(T)$ dependence (Feature 2). The U···U distances are long, making any ordering unlikely. Instead, the behavior may arise from spin fluctuations, where the intrinsic moment fluctuation effects outweigh thermal fluctuations. Spin fluctuations in other uranium compounds have manifested themselves as an upturn or broad maximum with saturation behavior in the $\chi(T)$ plot.[35] A similar feature in $Pd_3U_{0.9}S_4$ is attributed to magnetic ordering and partial U–S orbital hybridization.

Figure 8 shows the magnetization curves at 5 K for $Rb_2Pd_3US_6$ along the three crystallographic axes. Both the temperature and

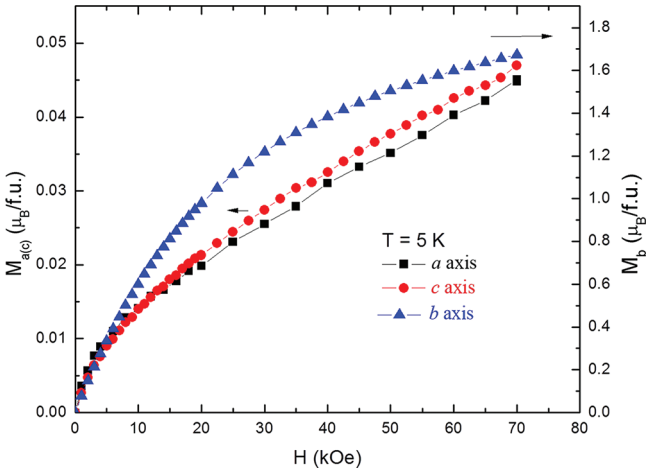

Figure 8. Magnetization plots of $Rb_2Pd_3US_6$. The left-hand *y* axis corresponds to the in-layer measurements, whereas the right-hand *y* axis corresponds to *b* axis measurements.

field dependence indicate uniaxial magnetism, with an easy *b* axis. Such behavior is consistent with the fact that U···U distances along the *b* axis are much longer, with correspondingly weaker 5*f*–5*f* electron interactions. CEF effects may also contribute to this anisotropy. An anisotropy field of 430 T was obtained from the intersection of a linear extrapolation of the *c* axis magnetization plot and an empirical curve fit of the *b* axis magnetization plot above 3 T (Figure 9). The anisotropy of the paramagnetic

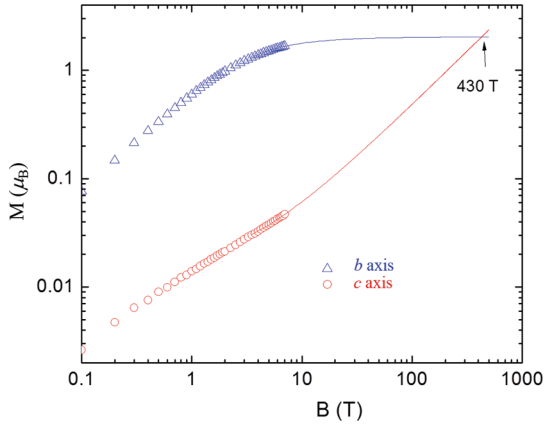

Figure 9. Extrapolations of the magnetization curves on a log–log plot. The intersection of the two curves corresponds to the anisotropy field.

susceptibility was also estimated from the difference in Weiss temperatures ($\Delta\theta$), giving a difference of about 200 K between the *a* or *c* and *b* axis measurements. The energy scales associated with the anisotropy field and $\Delta\theta$ are 0.025 and 0.017 eV, respectively.

■ ASSOCIATED CONTENT

Ⓢ Supporting Information

Crystallographic files in cif format for all compounds. This material is available free of charge via the Internet at http://pubs.acs.org

dx.doi.org/10.1021/ic2027048 | Inorg. Chem. 2012, 51, 4224–4230

AUTHOR INFORMATION

Corresponding Author

*E-mail: ibers@chem.northwestern.edu.

Notes

The authors declare no competing financial interest.

ACKNOWLEDGMENTS

The work presented was supported by the U.S. Department of Energy, Basic Energy Sciences, Chemical Sciences, Biosciences, and Geosciences Division and Division of Materials Science and Engineering Grant ER-15522. A portion of this work was performed at the National High Magnetic Field Laboratory, which is supported by NSF Cooperative Agreement No. DMR-0654118, by the State of Florida, and by the DOE. SEM analyses were conducted in the Electron Probe Instrumentation Center (EPIC) at the Northwestern University Atomic and Nanoscale Characterization Experimental (NUANCE) Center, supported by NSF-NSEC, NSF-MRSEC, Keck Foundation, the State of Illinois, and Northwestern University. Crystallographic data were collected at the IMSERC X-ray Facility at Northwestern University, supported by the International Institute of Nanotechnology (IIN). Use was made of the Magnetic and Low Temperature facility operated by the NSF-supported Northwestern University Materials Research Center.

REFERENCES

(1) Bugaris, D. E.; Ibers, J. A. *Dalton Trans.* **2010**, *39*, 5949−5964.
(2) Bugaris, D. E.; Choi, E. S.; Copping, R.; Glans, P.-A.; Minasian, S. G.; Tyliszczak, T.; Kozimor, S. A.; Shuh, D. K.; Ibers, J. A. *Inorg. Chem.* **2011**, *50*, 6656−6666.
(3) Bugaris, D. E.; Ibers, J. A. *Inorg. Chem.* **2012**, *51*, 661−666.
(4) Cody, J. A.; Ibers, J. A. *Inorg. Chem.* **1995**, *34*, 3165−3172.
(5) Yao, J.; Ibers, J. A. *Z. Anorg. Allg. Chem.* **2008**, *634*, 1645−1647.
(6) Cody, J. A.; Mansuetto, M. F.; Pell, M. A.; Chien, S.; Ibers, J. A. *J. Alloys Compd.* **1995**, *219*, 59−62.
(7) Sutorik, A. C.; Patschke, R.; Schindler, J.; Kannewurf, C. R.; Kanatzidis, M. G. *Chem.—Eur. J.* **2000**, *6*, 1601−1607.
(8) Daoudi, A.; Noël, H. *J. Solid State Chem.* **1985**, *60*, 131−134.
(9) Fujino, T.; Sato, N.; Yamada, K.; Masuda, H.; Wakeshima, M. *J. Alloys Compd.* **1998**, *271*−*273*, 452−455.
(10) Daoudi, A.; Noël, H. *J. Less-Common Met.* **1989**, *153*, 293−298.
(11) Oh, G. N.; Ibers, J. A. *Acta Crystallogr.* **2011**, *E67*, i9.
(12) Bugaris, D. E.; Ibers, J. A. *J. Solid State Chem.* **2008**, *181*, 3189−3193.
(13) Haneveld, A. J. K.; Jellinek, F. *J. Less-Common Met.* **1969**, *18*, 123−129.
(14) Sunshine, S. A.; Kang, D.; Ibers, J. A. *Mater. Res. Soc. Symp. Proc.* **1987**, *97*, 391−396.
(15) Suski, W.; Gibinski, T.; Wojakowski, A.; Czopnik, A. *Phys. Status Solidi A* **1972**, *9*, 653−658.
(16) Ellert, G. V.; Kuz'micheva, G. M.; Eliseev, A. A.; Slovyanskikh, V. K.; Morozov, S. P. *Russ. J. Inorg. Chem. (Transl. of Zh. Neorg. Khim.)* **1974**, *19*, 1548−1551.
(17) Bronger, W.; Rennau, R.; Schmitz, D. *Z. Anorg. Allg. Chem.* **1991**, *597*, 27−32.
(18) Grønvold, F.; Haraldsen, H.; Kjekshus, A. *Acta Chem. Scand.* **1960**, *14*, 1879−1893.
(19) Oh, G. N.; Choi, E. S.; Lu, J.; Ward, M. D.; Koscielski, L. A.; Ellis, D. E.; Ibers, J. A. Unpublished results.
(20) Bruker. *APEX2*, Version 2009.5-1; and *SAINT*, Version 7.34a; Data Collection and Processing Software; Bruker Analytical X-Ray Instruments, Inc.: Madison, WI, USA, 2009.
(21) Sheldrick, G. M. *SADABS*; Department of Structural Chemistry, University of Göttingen: Göttingen, Germany, 2008.
(22) Sheldrick, G. M. *Acta Crystallogr., Sect. A: Found. Crystallogr.* **2008**, *64*, 112−122.
(23) Gelato, L. M.; Parthé, E. *J. Appl. Crystallogr.* **1987**, *20*, 139−143.
(24) Spek, A. L. *PLATON*, A Multipurpose Crystallographic Tool; Utrecht University: Utrecht, The Netherlands, 2008.
(25) Sheldrick, G. M. *TWINABS*; University of Göettingen: Göettingen, Germany, 2008.
(26) Kanatzidis, M. G.; Poeppelmeier, K. R. *Prog. Solid State Chem.* **2007**, *36*, 1−133.
(27) Tams, G.; Müller-Buschbaum, H. *Z. Anorg. Allg. Chem.* **1992**, *617*, 19−22.
(28) Sonne, P.; Müller-Buschbaum, H. *Z. Anorg. Allg. Chem.* **1993**, *619*, 1004−1006.
(29) Huster, J.; Bronger, W. *J. Solid State Chem.* **1974**, *11*, 254−260.
(30) Oledzka, M.; Lee, J.-G.; Ramanujachary, K. V.; Greenblatt, M. *J. Solid State Chem.* **1996**, *127*, 151−160.
(31) Mitchell, R. H.; Ross, K. C.; Potter, E. G. *J. Solid State Chem.* **2004**, *177*, 1867−1872.
(32) Volkov, Y. F.; Tomilin, S. V.; Lukinykh, A. N.; Lizin, A. A.; Orlova, A. I.; Kitaev, D. B. *Radiochemistry (Transl. of Radiokhimiya)* **2002**, *44*, 319−325.
(33) Shannon, R. D. *Acta Crystallogr., Sect. A: Cryst. Phys., Diffr., Theor. Gen. Crystallogr.* **1976**, *32*, 751−767.
(34) Bronger, W.; Günther, O.; Huster, J.; Spangenberg, M. *J. Less-Common Met.* **1976**, *50*, 49−55.
(35) Sechovsky, V.; Havela, L. In *Handbook of Magnetic Materials*, 1st ed.; Buschow, K. H. J., Ed.; Elsevier: Amsterdam, 1998; Vol. *11*, pp 1−290.